Hindawi Publishing Corporation
International Journal of Photoenergy
Volume 2015, Article ID 747024, 9 pages
http://dx.doi.org/10.1155/2015/747024

Research Article

Enhanced Photocatalytic Activity of BiOBr/ZnO Heterojunction Semiconductors Prepared by Facile Hydrothermal Method

Xiangchao Meng,[1] Lingyun Jiang,[1] Weiwen Wang,[2] and Zisheng Zhang[1,2]

[1]*Department of Chemical & Biological Engineering, University of Ottawa, 161 Louis Pasteur, Ottawa, ON, Canada K1N 6N5*
[2]*College of Chemical Engineering, Qingdao University of Science & Technology, 53 Zhengzhou Road, Qingdao 266042, China*

Correspondence should be addressed to Zisheng Zhang; zzhang@uottawa.ca

Received 25 January 2015; Revised 28 April 2015; Accepted 29 April 2015

Academic Editor: Vincenzo Augugliaro

Hexagonal wurtzite pure ZnO and BiOBr-ZnO composites were synthesized by facile hydrothermal method. The amount of BiOBr as dopant was adjusted from 5 wt.% to 75 wt.%, and correspondingly the morphologies and crystal structures of the as-prepared composites were measured and discussed. Specifically, according to XRD patterns and SEM images, the main crystalline structure of ZnO was not destroyed after doping, but growth of ZnO crystals was inhibited by doping BiOBr. Meanwhile, the optical properties of the composites were measured by the diffuse reflectance spectra (DRS). The band gap of composites was also calculated using the classical Tauc equation and it was found to be around 3.0 eV. In the test of photocatalytic activation, the ZnO-BiOBr photocatalysts exhibited high photocatalytic efficiencies in the degradation of *Rhodamine B* (RhB) under visible-light irradiation. It was ascribed to not only the small size of crystalline, but also the reduction in the recombination rate of the photogenerated carriers for the enhancement effect of p-n heterojunction. This work sheds light on improving the photocatalytic performance by establishing the heterojunction and contributes to the development of a commercially competitive photocatalyst.

1. Introduction

Photocatalysis, one of the advanced oxidation processes (AOPs), has been vastly implemented in the remediation of environmental problems. In this promising technique, catalysts are stimulated by light with the generation of electron-hole pairs which would suffer from some secondary reactions to produce strong oxidative species such as $\bullet O_2^-$ and •OH. Organic pollutants in wastewater or polluted air could be completely mineralized by these species [1].

Since 1972, a variety of photocatalysts have been synthesized and implemented for environmental protection, such as TiO_2, CdS, and ZnO [2, 3]. Some critical drawbacks hinder their wide and commercial application in the industrial scale. Issues with the intrinsic properties of photocatalysts mainly include low visible-light-driven photocatalytic activity due to their wide band gaps and high recombination rates of photogenerated electron-hole pairs. Countermeasures were explored for these issues, including the modification of existing catalysts via noble metal deposition, doping, and so forth [4] and the fabrication of some novel materials with high visible-light photosensitivity [5].

In this work, BiOBr was chosen as the dopant and supported on ZnO to establish the p-n heterojunction which is supposed to possess an enhancement effect on the photocatalytic performance as reported in [6, 7]. Zinc oxide (ZnO), owing to its high stability, low cost, environmentally friendly properties, and easily controlled structure, has gradually drawn researchers' attention [8]. As a direct n-type semiconductor, the band gap of ZnO is about 3.2 eV, similar to TiO_2. This means that only irradiation with wavelengths lower than 400 nm, which is attributed to the UV-light range, could stimulate the photocatalytic reactions. Recently, as a promising approach to improve the photocatalytic activity, p-n heterojunction has provoked a heated point of research. The naturally generated bias in the p-n heterojunction is able to drive the opposite movement of the electrons and holes so as to significantly improve the separation rate and enhance the photocatalytic performance. Herein, the p-type semiconductor BiOBr, which can be activated under visible light due to its

relatively low band gap (2.7 eV), was doped onto ZnO in order to establish the type II starred alignment heterojunction [9]. The facile hydrothermal method was applied in the synthesis of BiOBr-ZnO composites. Compared with the only reported solvothermal method using CTAB as the solvent in [10], the operating procedures for the hydrothermal method were much easier and more environmentally friendly and showed a higher yield and purity [11]. To our knowledge, this is the first time in which the hydrothermal method was used to fabricate the BiOBr-ZnO heterojunction.

2. Experiment

2.1. Synthesis. In this experiment, zinc nitrate hexahydrate ($Zn(NO_3)_2{\cdot}6H_2O$, reagent grade) and sodium hydroxide (NaOH) were purchased from the Fisher Science Education, and potassium bromide (KBr, 99+% for spectroscopy, IR grade) and bismuth (III) nitrate pentahydrate ($Bi(NO_3)_3{\cdot}5H_2O$, 98% pure) were purchased from ACROS Company. All of the chemicals were of commercially available analytical grade and were used without further purification.

BiOBr/ZnO heterojunctions were synthesized by the facile hydrothermal method. Typically, 1.485 g of $Zn(NO_3)_2{\cdot}6H_2O$ and 0.4 g of NaOH (Zn/OH^- molar ratio of 1 : 2) were dissolved in 20 mL deionized water in a flask. After stirring for 10 minutes, white precipitates were formed and the solution was regarded as the precursor of ZnO. Similarly, a stoichiometric amount of KBr and $Bi(NO_3)_3{\cdot}5H_2O$ (Bi/Br molar ratio of 1 : 1) was dissolved in 80 mL deionized water. After stirring for 10 minutes, the precursor of BiOBr was synthesized. Then, these two precursors were mixed with continuous stirring for 20 minutes at room temperature. After that, the mixture was transferred into stainless steel Teflon-lined autoclaves and heated in the oven at 120°C for 12 h. Finally, the precipitates were collected, washed thoroughly with deionized water, twice, and dried at 50°C for 12 h. In this work, the doping amount of BiOBr was varied (5 wt.%, 10 wt.%, 15 wt.%, 25 wt.%, 50 wt.%, and 75 wt.%) to explore its effect on the photocatalytic performance of the composites.

2.2. Characterization. X-ray diffraction (XRD) patterns were recorded on Rigaku Ultima IV X-ray diffractometer using Cu-Kα radiation at 40 kV and 40 mA over the range of 2θ = 5°–90°. The morphology of the samples was observed with scanning electron microscopy (SEM), using a JEOL JSM-7500F field emission scanning microscope. UV-Vis spectroscopy was recorded on an Evolution 300 spectrophotometer equipped with a Labsphere diffuse reflectance accessory, with reflectance spectra of range 200–800 nm.

2.3. Photocatalytic Activity Test. The visible-light-driven photocatalytic activities of as-prepared pure ZnO and BiOBr/ZnO composites were measured by the degradation of *Rhodamine B* (RhB). As for the photocatalytic reactor, the light source was a 300 W halogen tungsten projector lamp (Ushio) with a 410 nm UV cut-off filter (Kenko Zeta, transmittance >90%) to ensure the wavelength attributed to the visible-light range. The distance between the irradiation source and the beaker was 10 cm, and the irradiation intensity was measured by a quantum meter (Biospherical QSL-2100, 400 nm < λ < 700 nm) to be 1.1 × 10^{-2} Einstein m^{-2} s^{-1}. In each batch, 0.1 g of the photocatalyst and 200 mL RhB aqueous solution with a concentration of 10 mg/m^3 were added into the beaker with a cooling jacket outside which could control the reaction temperature at around 25°C by a cooling/heating recirculating system. Before starting the photocatalytic reaction, the solution was magnetically stirred in the dark for 30 min to reach the adsorption-desorption equilibrium between the photocatalyst and dye RhB. Then, the solution was exposed to the visible-light irradiation under constant magnetic stirring. 1 mL of solution was collected and centrifuged before and after the dark reaction process and at every 10 min interval the concentration of which was tested by a Genesys 10-UV spectrophotometer (GENEQ Inc.) with the peak adsorption of RhB at 554 nm. A measured calibration curve was used to determine the RhB concentration from the absorbance shown in Figure 1.

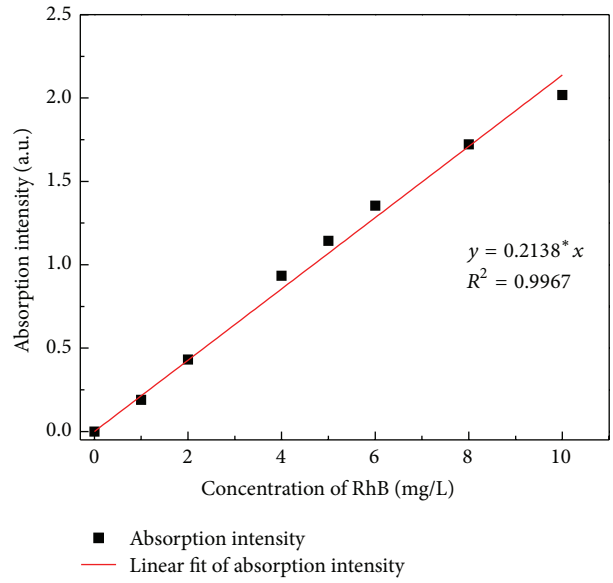

Figure 1: Calibration curve of plotting absorption intensities at various concentrations of RhB.

The linear relationship between the absorption intensity (A) and the concentration of RhB (c) could be expressed by

$$A = 0.2138 \times c \quad \left(R^2 = 0.9967\right). \tag{1}$$

The linear relationship could be ascribed to the dilute solution which fulfills the conditions of the Beer-Lambert law, in which the absorption intensity is proportional to the concentration of the solution. Based on this theory (2), the concentration of RhB could be determined by detecting

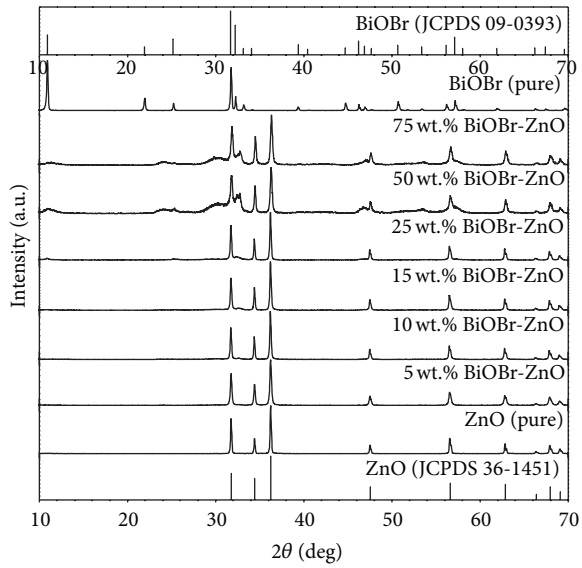

Figure 2: XRD patterns of pure ZnO and BiOBr, 5 wt.% BiOBr-ZnO, 10 wt.%-ZnO, 15 wt.% BiOBr-ZnO, 25 wt.% BiOBr-ZnO, 50 wt.% BiOBr-ZnO, and 75 wt.% BiOBr-ZnO composites synthesized by hydrothermal method.

the absorption intensity of the solution using a UV-Vis spectrometer:

$$\omega_{\text{Degradation efficiency}} = \frac{c_o - c_t}{c_o} \times 100\% = \frac{A_0/0.2138 - A_t/0.2138}{A_0/0.2138} \times 100\% = \frac{A_o - A_t}{A_o} \times 100\%. \quad (2)$$

3. Results and Discussions

3.1. XRD Analysis. The XRD patterns of pure ZnO and BiOBr, 5 wt.% BiOBr-ZnO, 10 wt.%-ZnO, 15 wt.% BiOBr-ZnO, 25 wt.% BiOBr-ZnO, 50 wt.% BiOBr-ZnO, and 75 wt.% BiOBr-ZnO composites synthesized by the hydrothermal method are shown in Figure 2. The characteristic peaks of both ZnO and BiOBr were in good agreement with the standard JCPDS cards (36-1451) and (09-0393) which suggested the crystal forms of hexagonal wurtzite ZnO and tetragonal crystal structure of BiOBr [15, 16]. No other impurity peaks were found, which indicated the high purity, and the sharp characteristic peaks proved high crystallinity of the samples. Meanwhile, with increasing amounts of BiOBr in the composites, the characteristic peaks of BiOBr came out gradually, especially the peaks at 10.9°, 25.2°, 31.7°, and 32.2° in good accordance with the (001), (101), (102), and (110) facets. It should also be noted that the characteristic peaks of ZnO were not influenced, which indicated that the crystal structure of ZnO was not destroyed by the BiOBr dopant.

3.2. SEM Analysis. SEM images of pure ZnO and BiOBr and 50 wt.% BiOBr-ZnO composites at low and high magnification are shown in Figure 3. The hourglass-like structure was found at about 3 μm in length and 0.5 μm in diameter for pure ZnO in Figures 3(a) and 3(b), which was novel, and a similar structure was reported in [12, 17, 18]. As for the formation process, ZnO with wurtzite structure initially nucleates a truncated hexagonal pyramid, and another unit would gradually grow on the (001) plane of it. Finally, the coupled hourglass-like structures were formed as shown in Figure 4. Pure BiOBr synthesized by the hydrothermal method had the nanoplate structure as shown in Figures 3(e) and 3(f). Meanwhile, by doping BiOBr in the composites, the regular structures were partially destroyed as shown in Figures 3(c) and 3(d). It exhibited many more defects in the polar planes on which some hollow sections were clearly observed. This kind of phenomenon could be caused by the Ostwald ripening process [19–21], which could be expressed as aiming to minimize the total Gibbs energy of crystallites. The smaller particles with higher interfacial energy, which lead to larger total Gibbs energy, are much more soluble and could be redisposed to form larger particles. In this work, the inner crystallites with normally small particle sizes were formed early at the nucleation stage and started dissipating in the aqueous solution, leaving the interior space and forming the hollow structure. It is supposed to be the reason that some cavities were found in Figures 3(c) and 3(d). It should also be noted that the size of the crystallite was decreased to less than 1 μm when doped by BiOBr compared with about 3 μm of the pure ZnO. When the amount of BiOBr in the composites increased to 50 wt.%, much more flake-like structures were found as shown in Figures 3(c) and 3(d), especially in the SEM images at high magnifications (i.e., Figure 3(d)). Apparently, the flake-like BiOBr was closely contacted with hourglass-like ZnO. The length and diameter of the coupled truncated hexagonal pyramid and the microsphere were both around 1 μm. Meanwhile, the proposed formation process of BiOBr-ZnO composites was schemed in Figure 4.

3.3. UV-Vis Diffuse Reflection Spectra (DRS). The optical properties of pure ZnO and BiOBr-ZnO composites were performed by UV-Vis diffuse reflection spectra (DRS), which were shown in Figure 5. A sharp decrease existed with increasing irradiation wavelengths greater than a specific value in both of them, which resulted from the band-gap transition. The following classical Tauc equation applies:

$$\alpha h\nu = A\left(h\nu - E_g\right)^n. \quad (3)$$

It should be mentioned that α, A, and n represent absorption coefficient, constant for semiconductors (equal to 1), and constant for type of semiconductor ($n = 2$ for indirect band-gap semiconductor and $n = 1/2$ for direct band-gap semiconductor, resp.) [22, 23]. It has been reported that ZnO is attributed to the n-type direct band-gap semiconductor as shown in Figure 6(a) [24] and BiOBr is attributed to the p-type indirect band-gap semiconductor as simulated and shown in Figure 6(b) [25]. So $n = 1/2$ was definitely implemented in the calculation of the band-gap value of pure ZnO, and in this

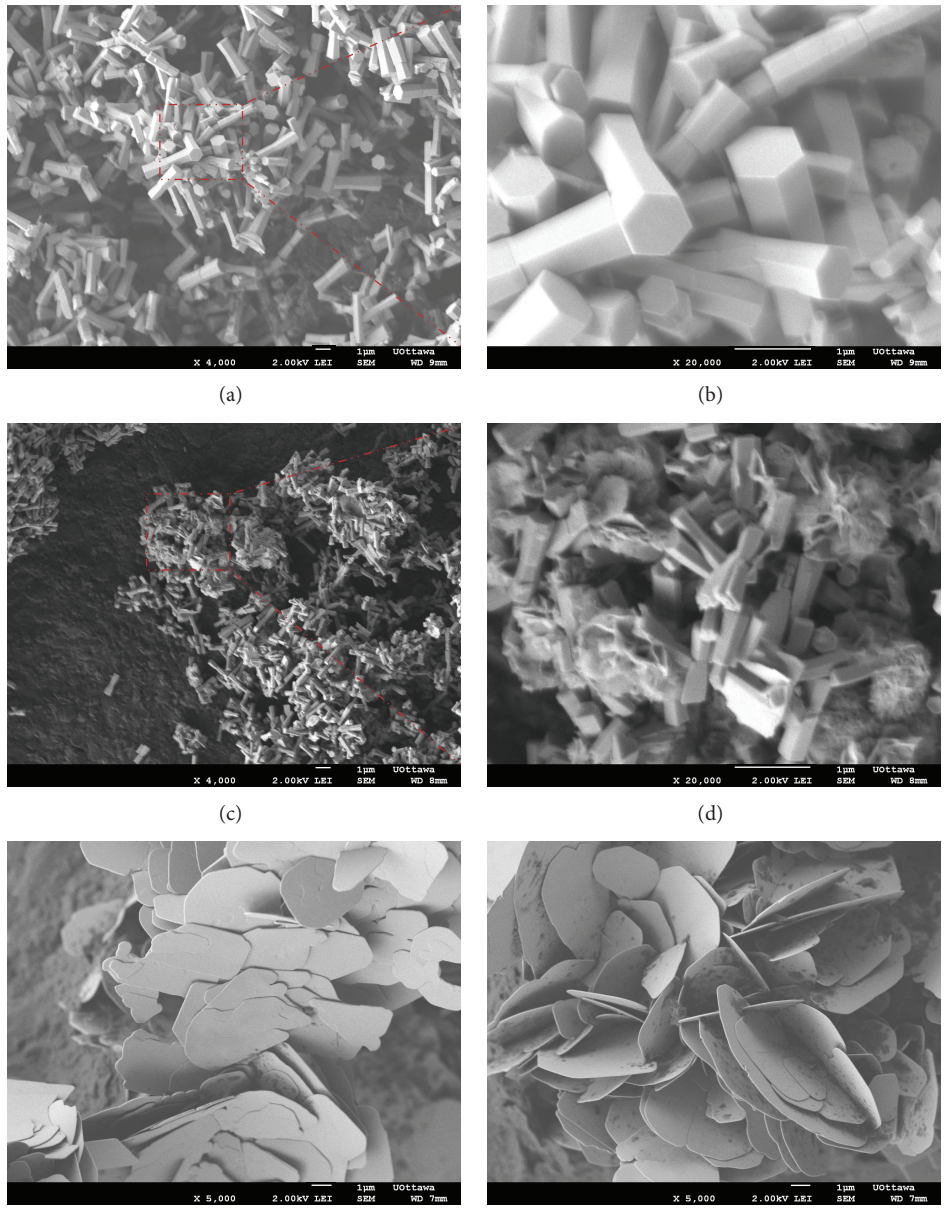

Figure 3: SEM images of pure ZnO at low (a) and high (b) magnification, 50 wt.% BiOBr-ZnO composites at low (c) and high (d) magnification, and pure BiOBr from different direction (e, f).

work $n = 2$ was assumed to calculate the band gap of BiOBr-ZnO composites. The illustration in Figure 5 demonstrated the band-gap values by plotting the tangent line. Band gap of the as-prepared pure ZnO was estimated at about 3.2 eV, in good accordance with other reported works [3]. Via doping BiOBr (50 wt.%) on ZnO, the band gap was narrowed to about 2.95 eV, which means that irradiation with wavelengths lower than 420 nm could induce the photocatalytic reaction.

3.4. Photocatalytic Activity. The photocatalytic activities of pure ZnO and BiOBr-ZnO composites were evaluated by the degradation of *Rhodamine B* under visible-light irradiation, results of which are shown in Figure 7. Two control tests were performed to account for the effects of photolysis and adsorption on the photocatalytic degradation of RhB. Results showed that 2.5% of the RhB reduction was caused by photolysis while 3.5% was caused by adsorption in the first 90 min of the control runs. An adsorption-desorption balance between the pollutants and the catalysts was obtained after 30 min. So, at the start of the photocatalytic process, pretreatment of the reaction system for 30 min in the dark was needed to minimize the adsorption effect. As for the photocatalytic performance, the degradation efficiency for pure ZnO was just 6% after 90 min. It might be due to the unsuitable band gap of ZnO under visible-light-induced conditions. In other words, ZnO was hard to stimulate by visible-light irradiation.

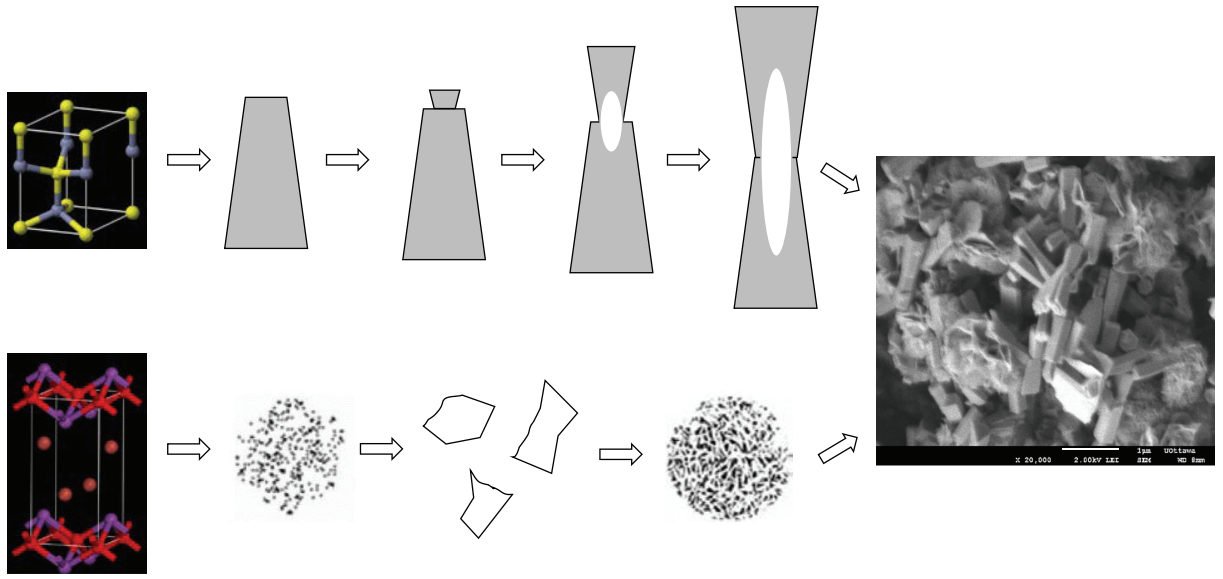

Figure 4: Possible formation processes of hourglass-like ZnO (adapted from [12]), flake-like microspheres (adapted from [13]), and the SEM image of final BiOBr-ZnO composite.

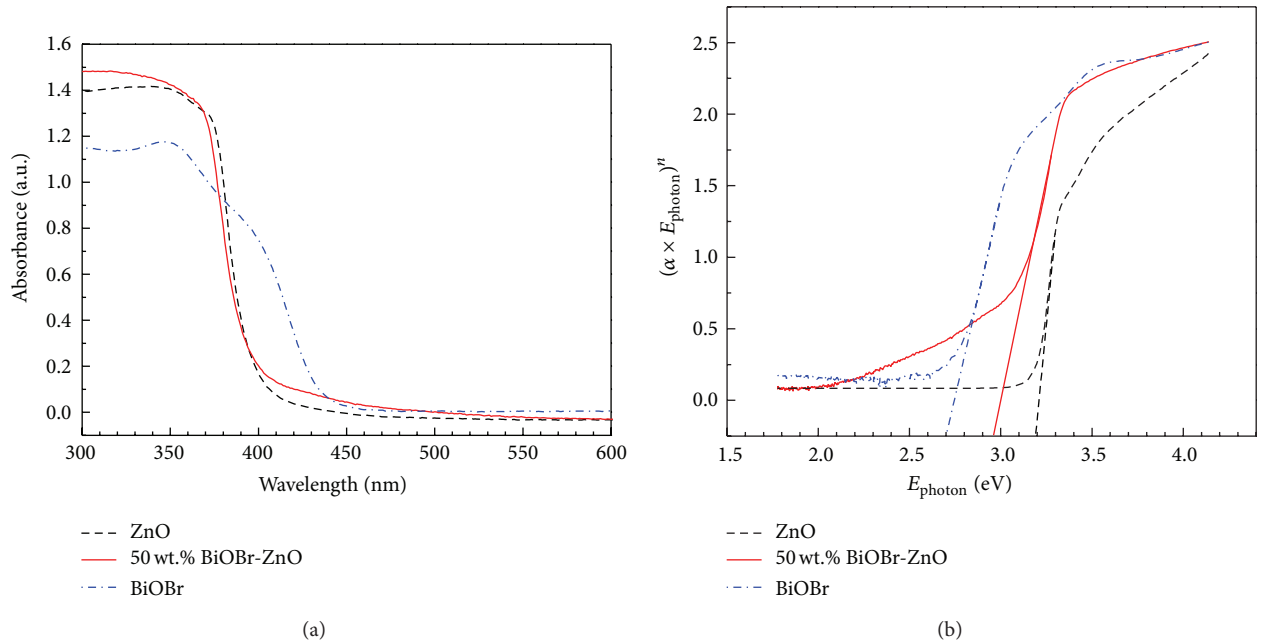

Figure 5: (a) Diffused reflectance spectra (DRS) and (b) $(\alpha * E_{photon})^n$-E_{photon} curves of pure ZnO and 50 wt.% BiOBr-ZnO composites.

By doping with BiOBr, the photocatalytic performances were significantly enhanced. Particularly, with increase of BiOBr in the composites from 5 wt.% to 50 wt.%, the degradation efficiency was improved from 6.5% to 97.0% in 90 min. The great improvement when doping with BiOBr was ascribed to both the high activity of BiOBr and the enhancement effect of the heterojunction, as the degradation efficiency of 50 wt.% BiOBr-ZnO was higher than that of pure BiOBr. However, when the amount of BiOBr reached 75 wt.% in composites, the degradation efficiency was reduced to 85.5% which was lower than that of 50 wt.% BiOBr-ZnO. It is because the heterojunctions were partially covered by excess BiOBr, which deteriorated its enhancement effect. To further explore the reaction kinetics, pseudo-first order theory was applied in this system via plotting $\ln(c_o/c)$ *versus* t shown in Figure 8 [26]. The perfect linear relationship proved the feasibility of using this model [27]. The reaction rate constant in each system was shown in Table 1. While BiOBr was below 50 wt.% in the composites, increasing the amount of BiOBr resulted in a higher reaction rate in the system. It decreased when the amount of BiOBr reached 75 wt.%. This means that the reaction rate was significantly enhanced with the BiOBr

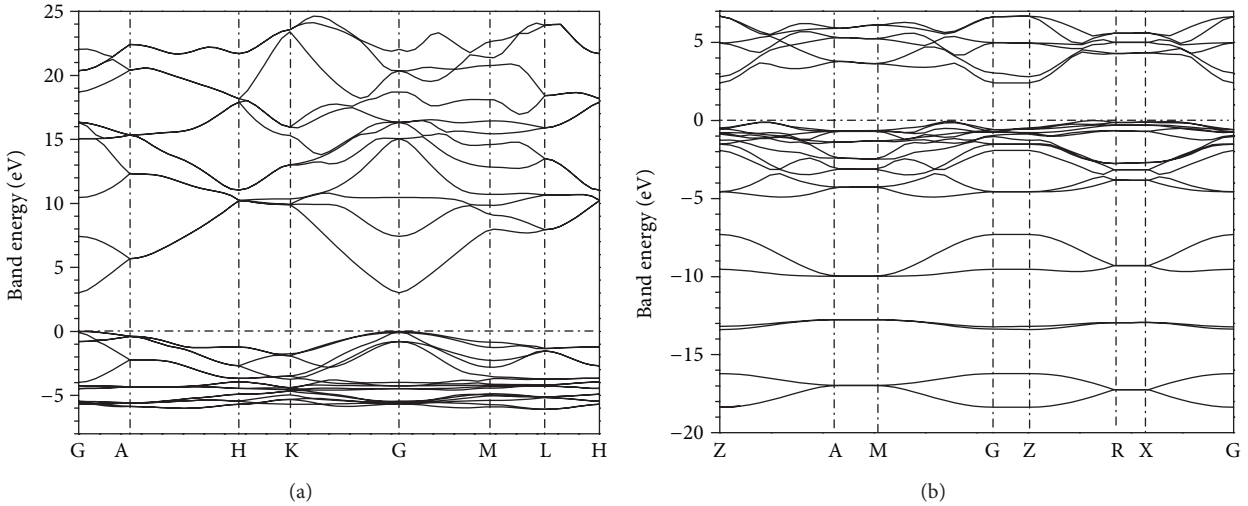

Figure 6: Band structure of ZnO (a) and BiOBr (b) (simulated by using Quantum Espresso [14]).

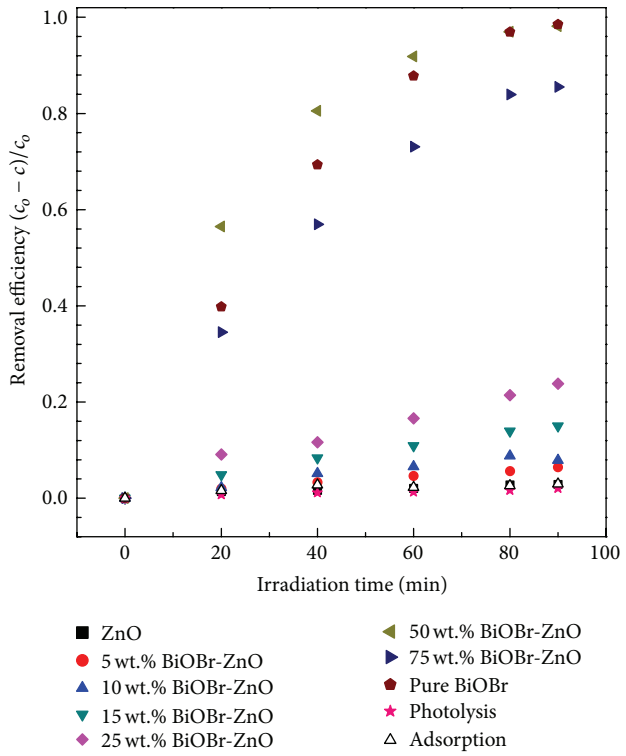

Figure 7: Photocatalytic degradation efficiencies of RhB as a function of time by loading various photocatalysts (dosage amount of photocatalysts: 0.5 g/L, initial concentration of RhB: 10 mg/L, and temperature of the system: 25°C).

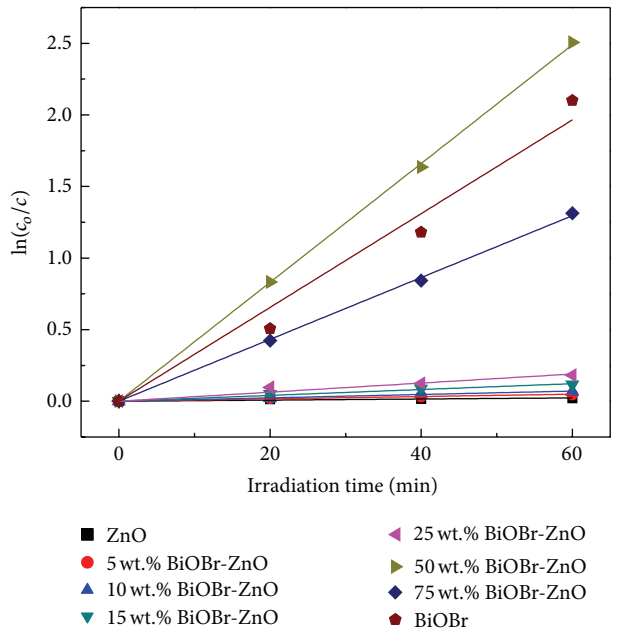

Figure 8: Kinetics for each photocatalytic process by plotting $\ln(c_o/c)$ *versus time*.

dopant compared with only implementing pure ZnO, and there exists an optimum value, in this work, at around 50 wt.% with the highest reactive activity.

The cut-off has been used to ensure that the wavelength of incident light was larger than 400 nm, so that only visible light contributes to the photocatalytic process. Figure 9 shows photocatalytic degradation efficiencies of the system with and without cut-off. After 20 min, the degradation efficiencies of RhB reached 56.5% and 68.1% in the system with and without cut-off, respectively. The difference indicates that the additional reactions due to the short wavelength radiations were significant for the illumination source used.

Furthermore, aiming to explore the effect of heterojunction, 50 wt.% BiOBr-ZnO composites were synthesized by the hydrothermal method and also by mechanical mixing to compare their effect on the degradation efficiency of RhB (Figure 10). It was clearly observed that the heterojunction enhanced the photocatalytic degradation process, with the degradation efficiency improving from 65.0% to 100% in

Table 1: Pseudo-first order reaction rate constant (k) for various processes, respectively.

Composites	k (10^{-3} min^{-1})	R^2
ZnO	0.39	0.9288
5 wt.% BiOBr-ZnO	0.82	0.9935
10 wt.% BiOBr-ZnO	1.18	0.9933
15 wt.% BiOBr-ZnO	2.05	0.9903
25 wt.% BiOBr-ZnO	3.17	0.9739
50 wt.% BiOBr-ZnO	4.15	0.9999
75 wt.% BiOBr-ZnO	2.16	0.9996
BiOBr	3.28	0.9875

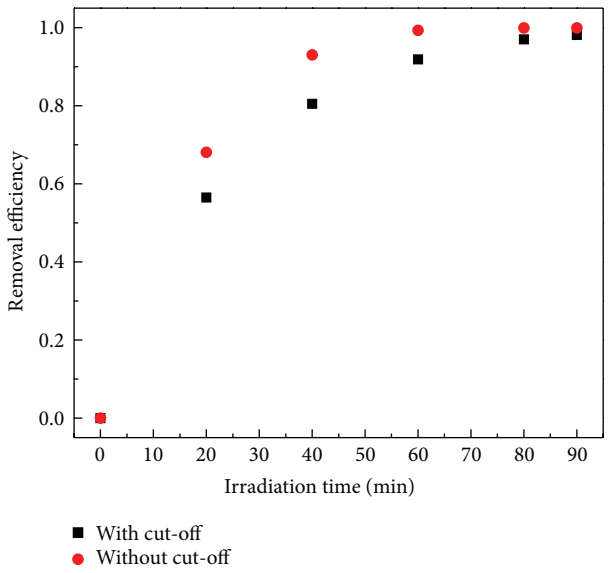

Figure 9: Photocatalytic degradation efficiencies of RhB with or without cut-off (dosage amount of photocatalysts: 0.5 g/L, initial concentration of RhB: 10 mg/L, and temperature of the system: 25°C).

90 min. The degradation efficiency of mechanically mixed composites was just approximately the mathematical mean of that when using pure BiOBr and ZnO. This phenomenon proved that each of them reacted individually and without enhancement by heterojunction. It could also be regarded as solid evidence to prove the successful establishment of heterojunction in the BiOBr-ZnO composites synthesized in this work.

4. Discussions and Conclusions

4.1. Mechanism of the Enhancement Effect. It has been reported that the E_{CB}, E_{VB} of p-type BiOBr and n-type ZnO were 0.8 eV, 0.85 eV and 3.5 eV, 3.9 eV, respectively, which has been depicted in Figure 11 [11]. The type of band alignments at the semiconductor interface is attributed to type II staggered alignment [9]. Naturally, an energy bias was generated to drive the separation of photogenerated electron-hole pairs [28]. Specifically, after irradiation stimulation, electrons and holes were produced by the photocatalytic effect. Driven by

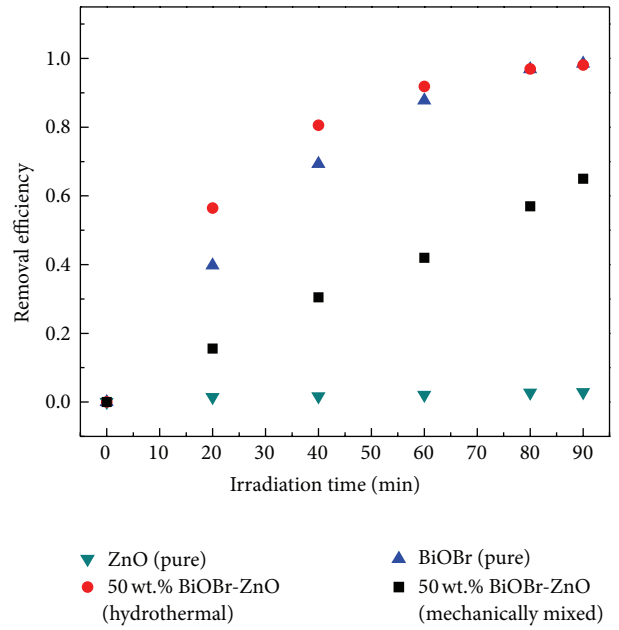

Figure 10: Removal efficiencies in degrading RhB by using 50 wt.% BiOBr-ZnO synthesized by hydrothermal method and mixed mechanically.

the bias generated at the depletion layer, electrons on the valence band of BiOBr could transfer to the valence band of ZnO; correspondingly, holes are accumulated on the conduction band of BiOBr. That kind of transfer, induced by p-n heterojunction, significantly prolongs the lifetime of electron-hole carriers and prevents the recombination of the electrons and holes. As a result, the performance of the BiOBr-ZnO photocatalysts was evidently enhanced. Moreover, the RhB was also probably excited by the irradiation due to the photosensitivity effect, and extra electrons were generated which could jump to the conduction band of either BiOBr or ZnO [29]. As for the photocatalytic degradation of RhB, the photogenerated electrons and holes suffer from some secondary reactions to produce some high oxidative radicals. To be more specific, electrons react with adsorbed O_2 to generate $\bullet O_2^-$, and holes could not only directly degrade RhB but also indirectly react with H_2O to produce the •OH which was regarded as the main species in the decomposition.

4.2. Conclusion. In summary, pure hexagonal wurtzite ZnO was successfully synthesized and doped with BiOBr to establish the p-n heterojunction by the facile hydrothermal method. Using the XRD and SEM analysis, the main crystal structure of ZnO was not destroyed and the hourglass-like structure was observed for the samples. As-prepared BiOBr-ZnO composites exhibited high photocatalytic activities in the degradation of RhB under visible-light irradiation. It has been significantly enhanced by the BiOBr dopant, and the possible mechanism of the enhancement effect by establishing p-n heterojunction was also explored and discussed. This work sheds light on a feasible approach in improving the photocatalytic activity via p-n heterojunction.

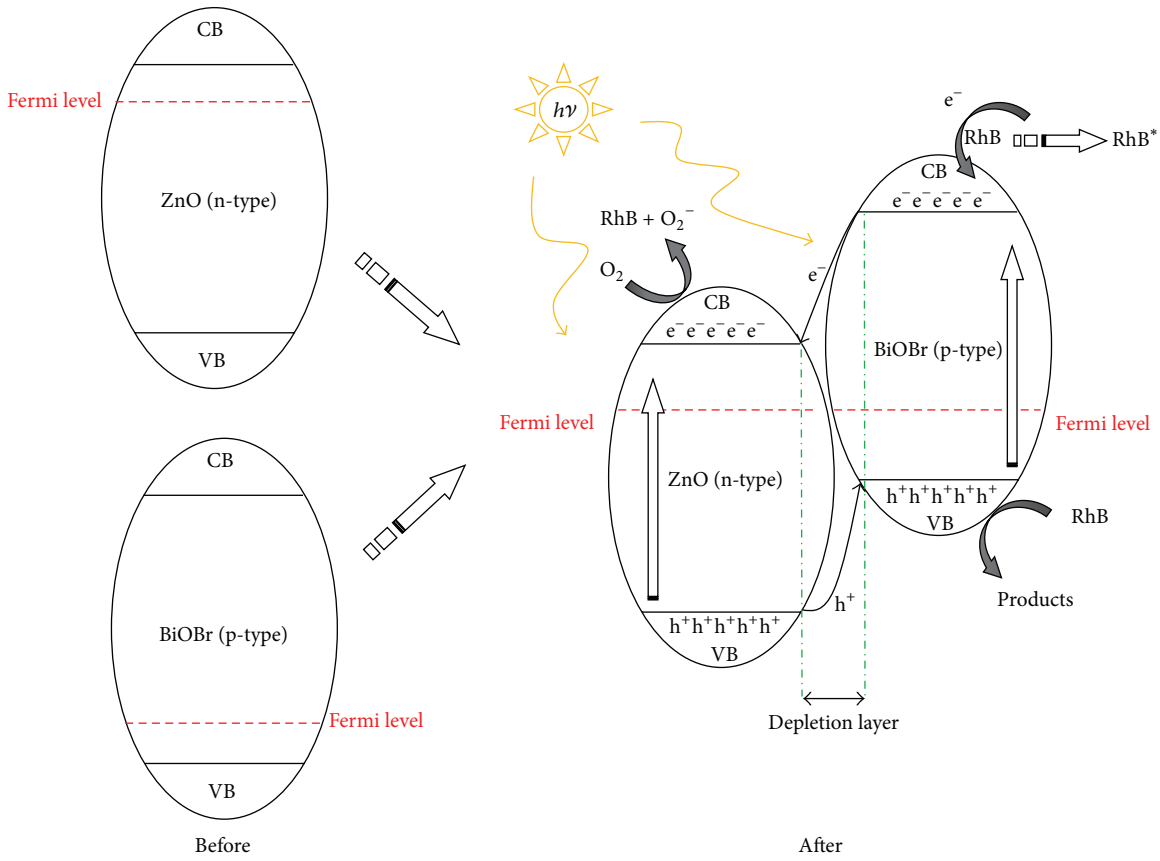

Figure 11: Diagram of band structure for BiOBr/ZnO composite and the possible photocatalytic degradation process.

Highlights

(1) BiOBr-ZnO p-n heterojunction was successfully synthesized by facile hydrothermal method.

(2) The amount and influence of dopant in the composite were optimized and discussed.

(3) Mechanism of enhancement effect by establishing heterojunction was explored and analyzed.

Conflict of Interests

The authors declare that there is no conflict of interests regarding the publication of this paper.

Acknowledgment

The authors hereby acknowledge the financial support of the work by the Natural Sciences and Engineering Research Council of Canada.

References

[1] A. L. Linsebigler, G. Lu, and J. T. Yates Jr., "Photocatalysis on TiO_2 surfaces: principles, mechanisms, and selected results," *Chemical Reviews*, vol. 95, no. 3, pp. 735–758, 1995.

[2] A. Fujishima and K. Honda, "Electrochemical photolysis of water at a semiconductor electrode," *Nature*, vol. 238, no. 5358, pp. 37–38, 1972.

[3] M. R. Hoffmann, S. T. Martin, W. Choi, and D. W. Bahnemann, "Environmental applications of semiconductor photocatalysis," *Chemical Reviews*, vol. 95, no. 1, pp. 69–96, 1995.

[4] S. G. Kumar and L. G. Devi, "Review on modified TiO_2 photocatalysis under UV/visible light: selected results and related mechanisms on interfacial charge carrier transfer dynamics," *The Journal of Physical Chemistry A*, vol. 115, no. 46, pp. 13211–13241, 2011.

[5] I. Tsuji, Y. Shimodaira, H. Kato, H. Kobayashi, and A. Kudo, "Novel stannite-type complex sulfide photocatalysts A^{I}_{2} -Zn-A^{IV}-S_4 (A^{I} = Cu and Ag; A^{IV} = Sn and Ge) for hydrogen evolution under visible-light irradiation," *Chemistry of Materials*, vol. 22, no. 4, pp. 1402–1409, 2010.

[6] J. Yu, S. Zhuang, X. Xu, W. Zhu, B. Feng, and J. Hu, "Photogenerated electron reservoir in hetero-p-n CuO-ZnO nanocomposite device for visible-light-driven photocatalytic reduction of aqueous Cr(vi)," *Journal of Materials Chemistry A*, vol. 3, pp. 1199–1207, 2015.

[7] Y. Peng, M. Yan, Q.-G. Chen, C.-M. Fan, H.-Y. Zhou, and A.-W. Xu, "Novel one-dimensional $Bi2O_3$-Bi_2WO_6 p-n hierarchical heterojunction with enhanced photocatalytic activity," *Journal of Materials Chemistry A*, vol. 2, no. 22, pp. 8517–8524, 2014.

[8] D. S. Bhatkhande, V. G. Pangarkar, and A. A. Beenackers, "Photocatalytic degradation for environmental applications—a

review," *Journal of Chemical Technology & Biotechnology*, vol. 77, no. 1, pp. 102–116, 2002.

[9] E. T. Yu, J. O. McCaldin, and T. C. McGill, "Band offsets in semiconductor heterojunctions," in *Solid State Physics*, E. Henry and T. David, Eds., pp. 1–146, Academic Press, 1992.

[10] H. Cheng, B. Huang, Z. Wang, X. Qin, X. Zhang, and Y. Dai, "One-pot miniemulsion-mediated route to BiOBr hollow microspheres with highly efficient photocatalytic activity," *Chemistry*, vol. 17, no. 29, pp. 8039–8043, 2011.

[11] F. Duo, Y. Wang, X. Mao, C. Fan, and H. Zhang, "Double Br sources fabrication and photocatalytic property of p-n junction BiOBr/ZnO composites for phenol removal," *Crystal Research and Technology*, vol. 49, no. 9, pp. 721–730, 2014.

[12] D. Zhang, J. Li, Y. Chen, Q.-S. Wu, and Y.-P. Ding, "One-pot preparation and enhanced photocatalytic and electrocatalytic activities of ultralarge Ag/ZnO hollow coupled structures," *CrystEngComm*, vol. 14, no. 20, pp. 6738–6743, 2012.

[13] X. Zhang, Z. Ai, F. Jia, and L. Zhang, "Generalized one-pot synthesis, characterization, and photocatalytic activity of hierarchical BiOX (X = Cl, Br, I) nanoplate microspheres," *The Journal of Physical Chemistry C*, vol. 112, no. 3, pp. 747–753, 2008.

[14] G. Paolo, B. Stefano, B. Nicola et al., "QUANTUM ESPRESSO: a modular and open-source software project for quantum simulations of materials," *Journal of Physics: Condensed Matter*, vol. 21, no. 39, Article ID 395502, 2009.

[15] L. Chen, R. Huang, M. Xiong et al., "Room-temperature synthesis of flower-like BiOX (X=Cl, Br, I) hierarchical structures and their visible-light photocatalytic activity," *Inorganic Chemistry*, vol. 52, no. 19, pp. 11118–11125, 2013.

[16] S. Baruah and J. Dutta, "Hydrothermal growth of ZnO nanostructures," *Science and Technology of Advanced Materials*, vol. 10, no. 1, Article ID 013001, 2009.

[17] K. X. Yao, R. Sinclair, and H. C. Zeng, "Symmetric linear assembly of hourglass-like ZnO nanostructures," *The Journal of Physical Chemistry C*, vol. 111, no. 5, pp. 2032–2039, 2007.

[18] D. Li, J. Wang, X. Wu, C. Feng, and X. Li, "Ultraviolet-assisted synthesis of hourglass-like ZnO microstructure through an ultrasonic and microwave combined technology," *Ultrasonics Sonochemistry*, vol. 20, no. 1, pp. 133–136, 2013.

[19] B. Liu and H. C. Zeng, "Symmetric and asymmetric ostwald ripening in the fabrication of homogeneous core-shell semiconductors," *Small*, vol. 1, no. 5, pp. 566–571, 2005.

[20] H. C. Zeng, "Synthesis and self-assembly of complex hollow materials," *Journal of Materials Chemistry*, vol. 21, no. 21, pp. 7511–7526, 2011.

[21] C. C. Yec and H. C. Zeng, "Synthesis of complex nanomaterials via Ostwald ripening," *Journal of Materials Chemistry A*, vol. 2, no. 14, pp. 4843–4851, 2014.

[22] C.-Y. Tsay, K.-S. Fan, S.-H. Chen, and C.-H. Tsai, "Preparation and characterization of ZnO transparent semiconductor thin films by sol-gel method," *Journal of Alloys and Compounds*, vol. 495, no. 1, pp. 126–130, 2010.

[23] D. C. Reynolds, D. C. Look, and B. Jogai, "Optically pumped ultraviolet lasing from ZnO," *Solid State Communications*, vol. 99, no. 12, pp. 873–875, 1996.

[24] A. Janotti and C. G. van de Walle, "Fundamentals of zinc oxide as a semiconductor," *Reports on Progress in Physics*, vol. 72, no. 12, Article ID 126501, 2009.

[25] J. Xia, J. Di, S. Yin et al., "Solvothermal synthesis and enhanced visible-light photocatalytic decontamination of bisphenol A (BPA) by g-C_3N_4/BiOBr heterojunctions," *Materials Science in Semiconductor Processing*, vol. 24, no. 1, pp. 96–103, 2014.

[26] X. Meng and Z. Zhang, "Synthesis, analysis, and testing of BiOBr-Bi_2WO_6 photocatalytic heterojunction semiconductors," *International Journal of Photoenergy*, vol. 2015, Article ID 630476, 12 pages, 2015.

[27] W. S. Kuo and P. H. Ho, "Solar photocatalytic decolorization of methylene blue in water," *Chemosphere*, vol. 45, no. 1, pp. 77–83, 2001.

[28] L. Kong, Z. Jiang, H. H. Lai et al., "Unusual reactivity of visible-light-responsive AgBr-BiOBr heterojunction photocatalysts," *Journal of Catalysis*, vol. 293, pp. 116–125, 2012.

[29] J. Zhuang, W. Dai, Q. Tian et al., "Photocatalytic degradation of RhB over TiO_2 bilayer films: effect of defects and their location," *Langmuir*, vol. 26, no. 12, pp. 9686–9694, 2010.